Cell Reports
Medicine

Report

Epothilones Improve Axonal Growth and Motor Outcomes after Stroke in the Adult Mammalian CNS

Graphical Abstract

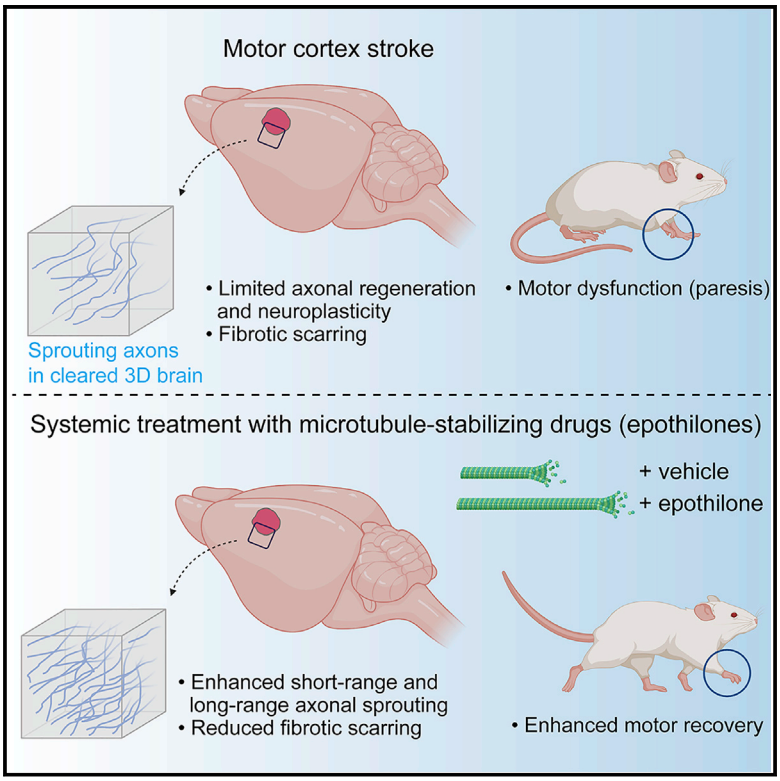

Highlights

- 3D visualization of axonal sprouting and remapping after cortical stroke in mice
- Systemic treatment with microtubule-stabilizing epothilones augments axon sprouting
- Epothilone treatment reduces fibrotic scar formation
- Epothilone treatment improves motor function with a wide therapeutic time window

Authors

Christof Kugler, Christian Thielscher, Bertrand A. Tambe, Martin K. Schwarz, Annett Halle, Frank Bradke, Gabor C. Petzold

Correspondence

gabor.petzold@dzne.de

In Brief

Kugler et al. use a 3D imaging approach in cleared whole-brain preparations to visualize axonal regeneration and cortical remapping in a mouse model of stroke. They find that the FDA-approved microtubule-stabilizing drugs, epothilones, augment novel peri-infarct connections, reduce fibrotic scarring, and improve skilled motor function, with a wide therapeutic time window.

Kugler et al., 2020, Cell Reports Medicine *1*, 100159
December 22, 2020
https://doi.org/10.1016/j.xcrm.2020.100159

CellPress

Cell Reports Medicine

CellPress
OPEN ACCESS

Report

Epothilones Improve Axonal Growth and Motor Outcomes after Stroke in the Adult Mammalian CNS

Christof Kugler,[1] Christian Thielscher,[1] Bertrand A. Tambe,[2] Martin K. Schwarz,[3] Annett Halle,[2] Frank Bradke,[4] and Gabor C. Petzold[1,5,6,*]

[1]Neurovascular Diseases Laboratory, German Center for Neurodegenerative Diseases (DZNE), 53127 Bonn, Germany
[2]Microglia and Neuroinflammation Laboratory, German Center for Neurodegenerative Diseases (DZNE), 53127 Bonn, Germany
[3]Experimental Epileptology and Cognition Research, Bonn University, 53127 Bonn, Germany
[4]Axon Growth and Regeneration Laboratory, German Center for Neurodegenerative Diseases (DZNE), 53127 Bonn, Germany
[5]Division of Vascular Neurology, Department of Neurology, University Hospital Bonn, 53127 Bonn, Germany
[6]Lead Contact
*Correspondence: gabor.petzold@dzne.de
https://doi.org/10.1016/j.xcrm.2020.100159

SUMMARY

Stroke leads to the degeneration of short-range and long-range axonal connections emanating from peri-infarct tissue, but it also induces novel axonal projections. However, this regeneration is hampered by growth-inhibitory properties of peri-infarct tissue and fibrotic scarring. Here, we tested the effects of epothilone B and epothilone D, FDA-approved microtubule-stabilizing drugs that are powerful modulators of axonal growth and scar formation, on neuroplasticity and motor outcomes in a photothrombotic mouse model of cortical stroke. We find that both drugs, when administered systemically 1 and 15 days after stroke, augment novel peri-infarct projections connecting the peri-infarct motor cortex with neighboring areas. Both drugs also increase the magnitude of long-range motor projections into the brainstem and reduce peri-infarct fibrotic scarring. Finally, epothilone treatment induces an improvement in skilled forelimb motor function. Thus, pharmacological microtubule stabilization represents a promising target for therapeutic intervention with a wide time window to ameliorate structural and functional sequelae after stroke.

INTRODUCTION

Stroke is a leading cause of death and disability worldwide.[1] Because causal treatment options are limited to the first few hours after the onset of ischemia,[2] the large majority of patients is ineligible for most therapies. Hence, there is an unmet need to establish novel strategies that promote the functional and structural recovery of neuronal connections in the subacute phase after stroke.

Interestingly, there is evidence for a limited capacity of surviving neurons after stroke to regenerate and re-establish connectivity by the initiation of plastic changes in peri-infarct and remote neuronal circuits that ultimately lead to a re-mapping of cortical areas.[3] In cortical stroke, axonal sprouting in the cortex bordering the infarct is one important mechanism underlying this compensatory structural and functional neuroplasticity. Thus, following an upregulation of axonal growth cone markers in peri-infarct neurons,[4] new short-range and long-range cortical and subcortical axonal projections arise from peri-infarct cortex within the first 3 weeks after ischemia[5–7] that remain stable long after stroke.[8] Importantly, the topography of these new projections is highly reproducible, consistent across species, and causally linked to recovery,[9] but their three-dimensional (3D) trajectories remain poorly described.

This limited capacity of the adult brain to partially reconnect damaged brain areas is hampered by physical or molecular impediments, including scar formation and the release of growth-inhibitory molecules.[9,10] This implies that substances that reduce scarring and promote axon growth may increase post-stroke axonal projections and functional outcomes. Indeed, it was found that pharmacological, viral, or transgenic approaches targeted against growth-inhibitory factors improve axonal sprouting and motor outcomes after experimental stroke.[7,11,12] However, the need for brain-topical delivery and the lack of regulatory approval for these approaches limit clinical translation.

An attractive alternative therapeutic option to overcome these difficulties is microtubule-stabilizing compounds, the epothilones.[13] These drugs induce axon growth by enabling the enhanced polymerization of microtubules to the tip of the axon[14] during development, but also in postnatal neurons exposed to growth-inhibitory factors such as Nogo and chondroitin sulfate proteoglycans.[15–17] Interestingly, microtubule-stabilizing drugs have decreased acute injury after a CNS injury.[15] Intriguingly, in a spinal cord injury model, the systemic administration of epothilone B (EpoB), a blood-brain barrier-permeable microtubule-stabilizing drug approved by the US Food and Drug Administration (FDA) for the treatment of

cancer,[18] increased regenerative axon outgrowth by microtubule polymerization and stabilization, reduced fibrotic scarring, and improved motor outcomes without obvious adverse effects.[17]

Therefore, the aim of this study was to test the effects of systemically administered EpoB and epothilone D (EpoD), an EpoB analog with a greater therapeutic index,[19] on newly formed short-range and long-range axonal projection patterns and motor outcomes in a mouse model of focal cortical stroke. We found that epothilones promote axonal growth, reduce scarring, and improve motor recovery, suggesting a novel option for stroke therapy with a potentially wide time window.

RESULTS

Axonal Regeneration after Stroke Quantified by 3D Imaging of Cleared Brains

Previous reports that measured axonal projections 2D in serial brain sections have shown that axons in peri-infarct brain tissue have the capacity to regenerate and form new connections with neighboring regions.[6,11] We aimed to investigate the extent and robustness of this stroke-induced axonal sprouting using an unbiased 3D imaging approach in cleared whole-brain preparations.[20] To model focal cortical stroke in mice, we used a photothrombosis model. In short, a reproducible ischemic infarct delineated by scar tissue is produced by the systemic administration of a photosensitizer followed by targeted irradiation of a defined cortical region.[21] This and similar models of cortical stroke have been used in previous studies to map axonal regeneration.[3,6] Using this technique in a thinned skull preparation, we induced focal cortical stroke in the forelimb area of the M1 primary motor cortex (Figure 1A). We then used anterograde and retrograde tracers to quantify connections formed by sprouting peri-infarct neurons after stroke. To this end, we injected the fluorescently labeled retrograde tracer cholera toxin B (CTb) into the premotor cortex (PMC) to back-label neurons that project from the infarcted motor cortex to the PMC (Figure 1A). In addition, we transduced neurons in the forelimb motor cortex anterior to the stroke site with adeno-associated virus (AAV) encoding for an anterograde enhanced green fluorescent protein (EGFP) tracer to label anterograde projections emanating from the primary motor cortex. Both tracers were injected 21 d after stroke induction (Figure 1A). Two weeks later (i.e., 5 weeks after infarct induction), isolated brains were rendered transparent by whole-brain organic solvent-based clearing (Figure 1B).[22] Subsequently, anterograde and retrograde M1-PMC neuronal connections were 3D imaged and quantitively mapped in defined areas medial, lateral, and anterior to the infarct (Figure 1C). While control mice that had undergone a sham-stroke procedure showed robust retrograde labeling from PMC to M1 (Figures 1D and 1E; Video S1), we found that mice with a cortical stroke displayed a reduction of >60% of these connections anterior, medial, and lateral to the infarct (anterior, 35% compared to sham; medial, 20% compared to sham; lateral, 42% compared to sham; Figures 1D and 1E; Video S2). Similarly, anterograde connections between M1 and the PMC were strongly reduced in areas anteromedial and posterolateral to the infarct in mice after cortical stroke compared to sham-treated control mice (anteromedial, 62% compared to sham; posterolateral, 70% compared to sham; Figures 1F–1H). However, we also detected new projections that emerged from peri-infarct areas into the anterolateral motor and somatosensory (S1) cortex (anterolateral motor cortex, 326% compared to sham; S1, 128% compared to sham; Figures 1F–1H and S1). Hence, we subsequently aimed to investigate whether the growth of these novel connections can be stimulated pharmacologically.

Epothilones Augment Plastic Regeneration of Peri-infarct Axons after Stroke

To investigate whether epothilones augment the regenerative potential of sprouting peri-infarct axons, we tested the effects of EpoB and EpoD on this stroke-induced increase in neuroplasticity, as well as on peri-infarct fibrotic scarring and behavioral outcomes. Mice were treated systemically (by intraperitoneal injection) with either drug or vehicle 1 and 15 days after infarct induction, and neuronal re-mapping and motor outcome were quantified by blinded analysis (Figure 2A). No changes were evident in mice undergoing a sham stroke procedure that were treated with EpoB or EpoD, and vehicle alone also induced no changes in projection patterns after stroke (data not shown).

We found that the stroke-induced plastic "redistribution" of axonal connection patterns—a reduction in anteromedial M1-PMC and posterolateral connections, and an increase in anterolateral motor and M1-S1 connections—occurred in epothilone-treated animals. Remarkably, however, both treatments, EpoB in particular, resulted in a higher number of anterograde and retrograde connections after stroke. Specifically, treatment with EpoB more than doubled retrograde axonal projections between M1 and PMC anterolateral to the infarct and increased these projections by >50% medial to the infarct compared to vehicle-treated control mice (anterior, 231% compared to vehicle; lateral, 191% compared to vehicle; medial, 158% compared to vehicle; Figure 2B). Moreover, EpoB also increased by >50% the anterograde connections from peri-infarct cortex into anterolateral motor and somatosensory cortices (153% compared to vehicle; Figures 2C–2F; Video S3), and we also found a stronger reduction in anteromedial connections after stroke in mice treated with EpoB (Figure 2D).

As the anterograde tracer appeared as linear structures resembling intact axons as well as discontinuous dot-like structures, we also limited our analysis to continuous linear structures. These analyses confirmed that anteromedial M1-to-PMC projections were reduced in mice treated with EpoB or vehicle after stroke, but increased anterolateral to the infarct in these groups compared to sham (Figures S2A–S2C).

Axon regrowth initiated shortly after stroke. Confocal imaging revealed that EpoB treatment led to higher axonal coverage already at 3 days after stroke, whereas EpoD increased axonal coverage only after 7 days (Figures S2D and S2E). Moreover, we found that, paralleling the epothilone-induced increase in axon density after stroke, more axons were myelinated in mice treated with EpoB or EpoD after stroke compared to vehicle-treated mice at 14 days after stroke (Figures S2F and S2G); these axons also formed axon initial segments and nodes of Ranvier (Figures S2H and S2I).

CellPress
OPEN ACCESS

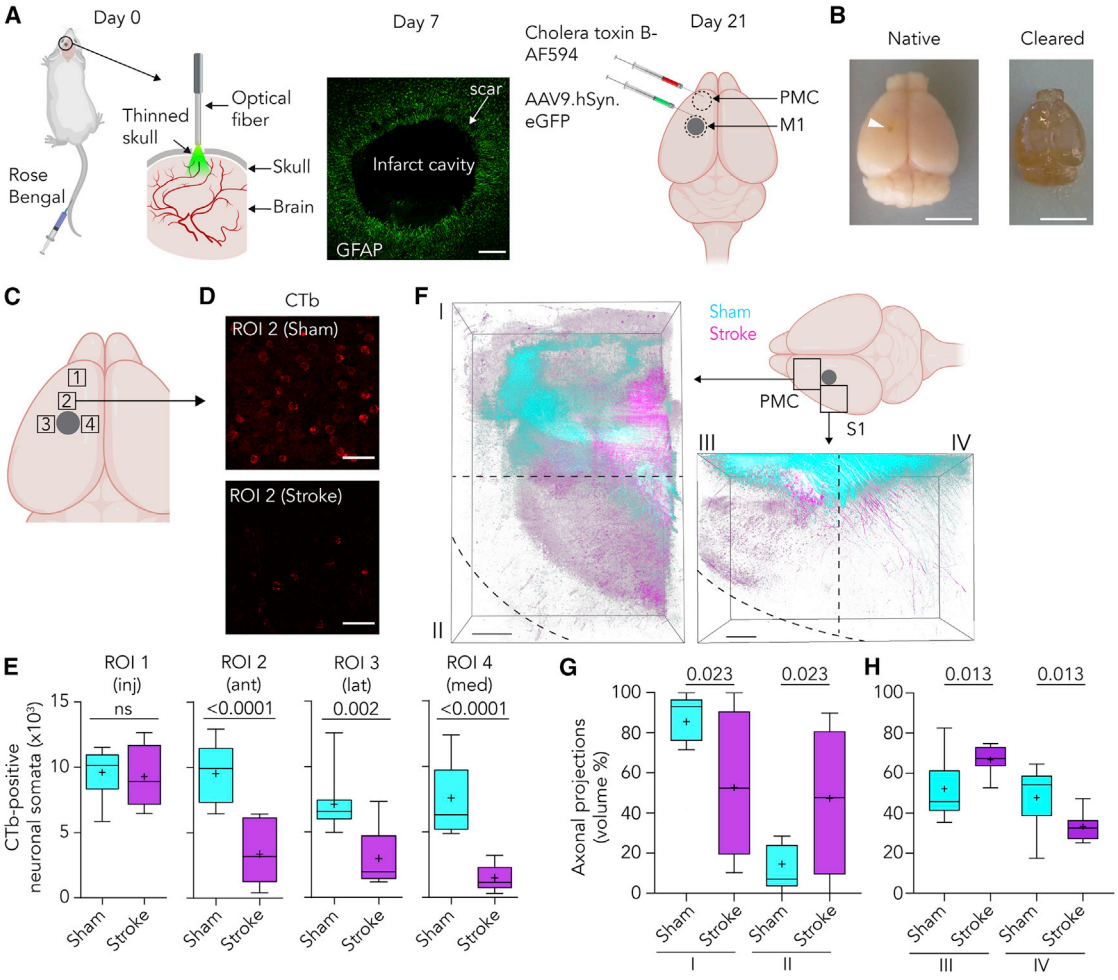

Figure 1. Axonal Re-mapping after Cortical Stroke

(A) We induced photothrombotic stroke through the thinned skull, resulting in an infarct surrounded by scar tissue (stained with glial fibrillary acidic protein [GFAP], scale bar, 300 μm). At day 21, fluorescent cholera toxin B (CTb) and AAV9 encoding for hSyn.eGFP were injected into the primary motor cortex (M1) and the premotor cortex (PMC).

(B) Whole-brain organic solvent-based brain clearing (arrowhead, infarct area; scale bars, 1 mm).

(C) Retrograde CTb labeling was analyzed in 4 regions of interest (ROIs): the injection site (1) and ROIs anterior (2), lateral (3), and medial (4) to the infarct.

(D and E) No differences were seen at the injection site, whereas stroke led to a reduction in retrograde labeling in all other areas (n = 10 stroke versus n = 10 sham animals, Mann-Whitney test; scale bars, 50 μm; images in D show CTb-labeled cells in ROI 2 in sham versus stroke).

(F–H) Anterograde EGFP labeling was assessed in PMC and somatosensory cortex (S1) anterior and medial to the infarct, and these areas were divided into ROIs I–IV (summation images of all animals, depicted as color-coded maximal intensity z projections). Stroke led to a reduction in anterograde connections in ROIs I and IV, but also induced new connections in ROIs II and III (i.e., in anterolateral motor and somatosensory cortex; n = 10 stroke versus n = 10 sham animals, Mann-Whitney test; scale bars, 300 μm).

See also Figure S1.

Epothilones Reduce Peri-infarct Fibrotic Scar Formation

Microtubule-stabilizing drugs also reduce fibrotic scarring.[16,17] Hence, we tested the effects of EpoB and EpoD on fibrotic scar formation in the infarct rim. Immunohistochemistry revealed that EpoB reduced fibrotic scarring in the peri-infarct cortex 14 d after stroke by approximately one-third compared to animals that had undergone stroke alone, as quantified by laminin and fibronectin immunoreactivity (laminin, 63% compared to vehicle; fibronectin, 74% compared to vehicle; Figures 3A and 3B). No significant changes were seen in mice treated with EpoD (data not shown). Moreover, no differences were seen in astrogliotic scar formation and microglial activation for all of the treatments (Figures S3A–S3F). In addition, we did not detect any changes in branch number, total process length, and the spanned volume of astrocytes and microglia in mice treated with EpoB compared to vehicle 3, 7, and 14 days after stroke (Figures S3A–S3F). The number of peri-infarct neuronal somata 3, 7, and 14 days after stroke was not altered by treatment (Figure S3G), arguing against effects on cell survival; the infarct volume was similar in all of the groups (Figure S3H).

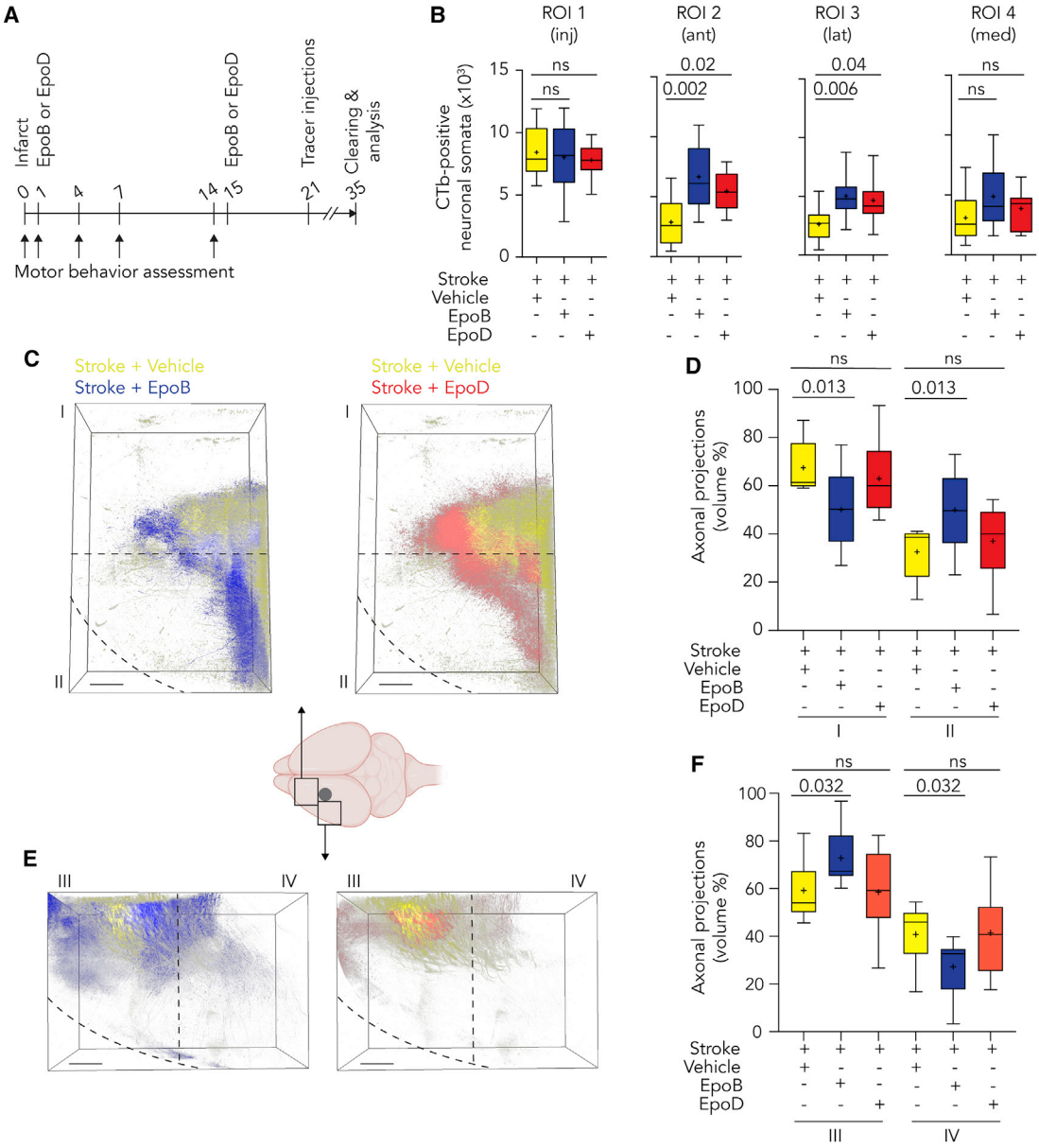

Figure 2. Epothilone B and D Promote Stroke-Induced Axonal Neuroplasticity

(A) Experimental timeline.

(B) EpoB (n = 15) and EpoD (n = 15) treatments both induced significantly more retrograde connections from regions lateral and anterior to the infarct compared to animals treated with vehicle (n = 9) after stroke (Kruskal-Wallis test followed by Dunn's multiple comparisons test).

(C–F) Analysis of anterograde axonal connections showed that EpoB also induced significantly more connections emanating from areas anterolateral from the stroke region (summation images depict color-coded maximal intensity z projections; stroke and vehicle, n = 9 mice; stroke and EpoB, n = 15 mice; stroke and EpoD, n = 15 mice; Kruskal-Wallis test followed by Dunn's multiple comparisons test; scale bars, 300 μm).

See also Figure S2.

Epothilones Increase Long-Range Motor Tract Connections after Stroke

We next investigated the effects of EpoB and EpoD on long-range corticonuclear connections. To this end, we quantified the coverage of axons within the ipsilateral brainstem red nucleus positive for the fluorescent anterograde viral tracer that had been injected into the peri-infarct motor cortex. As expected, stroke led to a reduction in the spatial coverage of corticonuclear axons within the red nucleus (34% compared to sham; Figures 3E and 3F). Importantly, EpoB treatment after stroke almost doubled axon density in the red nucleus compared to vehicle-treated mice after stroke (188% compared to stroke and vehicle, and 63% compared to sham; Figures 3E and 3F), whereas only minor effects were seen after EpoD treatment (128% compared to stroke and vehicle, and 43% compared to sham; Figures 3E and 3F). Similar effects of stroke and

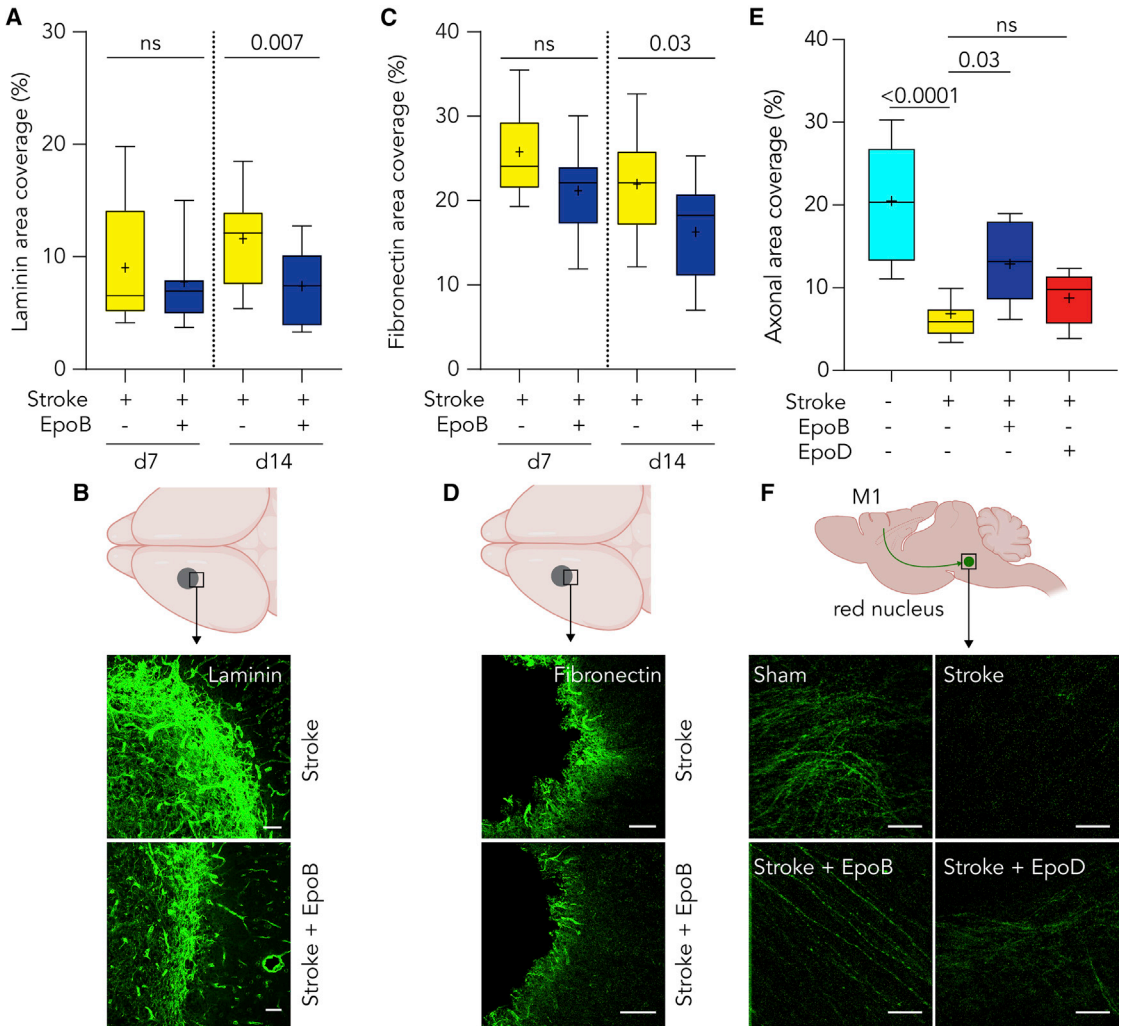

Figure 3. Epothilones Modulate Peri-infarct Scarring after Cortical Stroke and Increase Long-Range Connectivity

(A–D) EpoB strongly reduced peri-infarct scarring, assessed by laminin and fibronectin immunohistochemistry, 14 days after stroke induction (n = 15 mice per group; Mann-Whitney test for each time point; drawing indicate areas of investigation; images show representative examples; scale bars, 200 μm).

(E and F) Long-range projections from peri-infarct motor cortex were assessed by quantifying $EGFP^+$ axons in the red nucleus within the ipsilateral brainstem. Stroke induced a strong reduction of these connections, but EpoB significantly increased axonal area coverage (n = 10 mice per group; Kruskal-Wallis test followed by Dunn's multiple comparisons test; images show representative examples; scale bars, 50 μm).

See also Figures S3, S4A, and S4B.

epothilone treatment were also evident in the brainstem facial nucleus (Figures S4A and S4B).

Epothilone Treatment Improves Motor Outcomes after Stroke

Finally, we investigated the effects of epothilones after stroke on motor outcomes. Motor cortex stroke produces reproducible deficits in skilled contralateral forelimb use.[23] Hence, we tested skilled forelimb function by quantifying the foot faults of mice placed on an elevated grid. This test was performed 1 day before stroke or sham procedure, respectively, and repeated at defined intervals after stroke. As expected, while mice undergoing sham surgery showed very few foot faults, animals after stroke showed approximately three times more foot faults of the contralateral forepaw (Figures 4A and 4B). Importantly, these deficits were strongly ameliorated by epothilones. Specifically, EpoB almost halved the number of foot faults 4, 7, and 14 days after stroke (50%, 62%, and 61% compared to vehicle for each time point, respectively; Figure 4C). Remarkably, the improvement was robust enough in EpoB-treated mice that the absolute number in foot faults at 14 days had almost returned to baseline—that is, to the levels before stroke induction (Figure 4C). EpoD reduced foot faults by approximately one-third 4 and 7 days after stroke (60% and 67% compared to vehicle for each time point, respectively; Figure 4C), but approached sham levels at day 14 (Figure 4C). As expected, no differences were seen in skilled

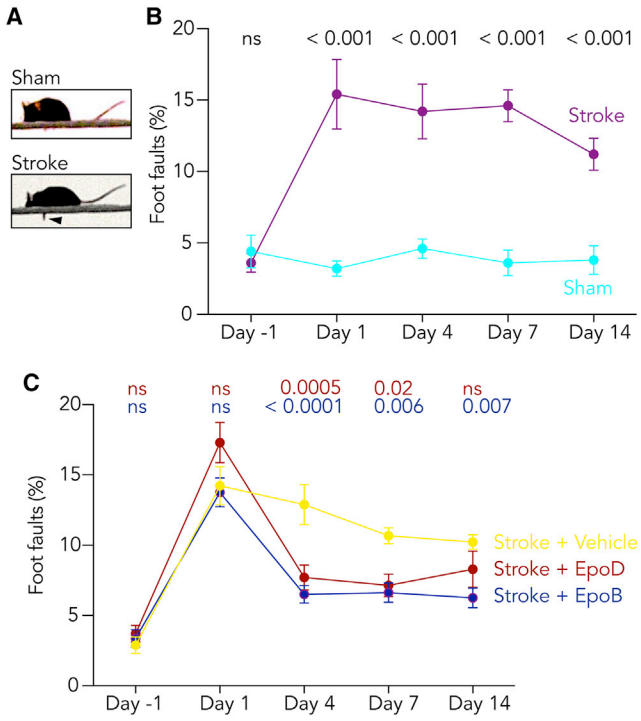

Figure 4. Epothilones Improve Motor Outcomes after Cortical Stroke

(A and B) Images show representative examples of successful grid walk ambulation in a sham-treated animal and a foot fault in an animal after stroke (arrowhead). Motor outcome was assessed for 14 days after stroke induction by testing skilled forelimb function using the elevated grid walk test. Whereas mice performed similarly before infarct induction (day −1), cortical stroke worsened skilled motor function of the contralateral forelimb, assessed by the foot fault frequency, until 14 days after stroke (n = 10 mice per group; repeated-measures 2-way ANOVA followed by Bonferroni's multiple comparisons test).

(C) EpoB and EpoD both improved skilled motor function of the contralateral forelimb compared to vehicle-treated animals after stroke (stroke and vehicle, n = 9; stroke and EpoB, n = 16; stroke and EpoD, n = 14; repeated-measures 2-way ANOVA followed by Bonferroni's multiple comparisons test).

See also Figures S4E and S4F.

contralateral hindpaw use, as the cortical representation of hindpaw function was outside the ischemic region in our model (Figures S4C and S4D).

DISCUSSION

Current approaches to treat stroke are limited to the first few hours. Here, we found that microtubule-stabilizing drugs, the epothilones, promote axonal growth after cortical stroke within a large time window, ultimately leading to improved skilled limb function. Thereby, our study reveals that epothilones hold promise for clinical use after stroke.

Our findings indicate that at least two mechanisms, augmentation of peri-infarct axon regeneration by microtubule stabilization and reduced fibrotic scarring, contribute to the observed therapeutically relevant effects. The limited capacity of the adult brain to reconnect damaged brain areas is hampered by physical or molecular impediments that occur simultaneously, such as scar formation and the release of growth-inhibitory molecules.[9,10] Substances such as epothilones, which enhance axon growth and reduce fibrotic scarring, may be superior to compounds that are selective for single mechanistic targets. Importantly, the neutral effect of epothilones on glial fibrotic scar formation observed here may also be a beneficial property as reduction of the astroglial scar may worsen axonal outgrowth after stroke.[24]

Moreover, the epothilone-induced plastic restoration and preservation of cortical projections as well as long-range motor tract connections led to meaningful improvements in skilled motor function, underlining the potential of peri-infarct neuroplasticity as a target in preclinical drug development. Importantly, some microtubule-stabilizing drugs, including epothilones, have been approved by the FDA and other agencies for different indications and have been shown to penetrate the brain after systemic administration,[25] indicating that epothilones and other compounds may be tested in clinical drug repurposing trials for acute stroke.

Importantly, the effects on axonal growth and motor outcome were evident when treatment was initiated even 24 h after stroke onset, indicating a much wider time window compared to currently approved therapies, which are mostly limited to the first 4–6 h.[2] Interestingly, our data suggest that the behavioral effects of EpoB are superior to those of EpoD, which may be related to the different pharmacokinetics of EpoB and EpoD. In particular, the maximal tissue concentration and half-life of EpoD are significantly shorter in brain and plasma compared to EpoB,[19] indicating that EpoB may be better suited to chronically modulate axon regeneration after ischemic stroke. Of note, our data also indicate that these therapeutic effects begin to appear several days after ischemia. Although the earliest starting point at which axonal regeneration commences after stroke is not clearly established, several studies have suggested that axonal sprouting may start as early as 2–3 days after stroke.[26,27] Interestingly, live imaging of axon regeneration both in cell culture and *in vivo* showed that pharmacological microtubule stabilization enables axon growth within a few hours,[17] which is compatible with a mechanistic link between enhanced axon regeneration and improved motor outcomes at early time points. Thus, we envision that microtubule stabilization speeds up this process of sprouting and integration within cerebral networks.

Finally, on a technical level, we propose that the quantification of axonal short-range and long-range re-mapping into neighboring and subcortical target regions, and the effective testing of pharmacological candidates in preclinical trials, is greatly facilitated by our unbiased 3D-imaging approach in cleared whole-brain preparations.

In summary, pharmacological microtubule stabilization with epithilones or other substances may represent a novel therapeutic option, with a potentially wide time window to ameliorate detrimental sequelae after stroke.

Limitations of Study

It is well established that the re-mapping of cortical projections is mediated by active and directionally specific axonal outgrowth of surviving neurons,[9] an effect specifically targeted by epothilones.[17] However, we did not formally characterize the molecular

identity of sprouting axons in our study, and hence it remains to be investigated on a molecular level whether enhanced regeneration or increased survival underlie these therapeutic effects. As additional steps toward clinical testing, it will also be important in future studies to test different dosing regimens, to investigate the effects of epothilones on aged and comorbid animals, and to conduct confirmatory multi-center preclinical trials.[28] Moreover, while both epothilones increased retrograde anteromedial connections after stroke, the stroke-induced reduction of anterograde anteromedial connections was also enhanced by EpoB. Such pruning, which is typical for functional integration during development and reintegration into damaged circuits,[29] may help to strengthen the recovery of epothilone-treated animals, but the exact relation between anatomical integration and functional recovery is a fundamental question to be addressed in the future. In addition, although epothilones improved motor function, their effects on more complex and translationally relevant motor tests remain to be determined. Although our analysis did not reveal any effects on microglial reactivity, it will also be important to determine whether microglial motility and other inflammatory mechanisms are modulated by epothilones. Finally, future studies may also elucidate whether these effects can be generalized to other stroke types such as larger infarct sizes or hemorrhagic stroke.

STAR★METHODS

Detailed methods are provided in the online version of this paper and include the following:

- KEY RESOURCES TABLE
- RESOURCE AVAILABILITY
  - Lead Contact
  - Materials Availability
  - Data and Code Availability
- EXPERIMENTAL MODEL AND SUBJECT DETAILS
- METHOD DETAILS
  - Photothrombotic stroke model
  - Motor behavior
  - Drug treatment
  - Intracranial injections
  - Whole-brain clearing
  - Immunohistochemistry
  - Confocal and two-photon microscopy
- QUANTIFICATION AND STATISTICAL ANALYSIS

SUPPLEMENTAL INFORMATION

Supplemental Information can be found online at https://doi.org/10.1016/j.xcrm.2020.100159.

ACKNOWLEDGMENTS

We thank Theresa Schulte, Jan Peter, Christoph Moehl, Kevin Keppler, Sanjeev Kaushalya, Cordula Rakers, and Andrea Delekate for their technical assistance and Barbara Schaffran for discussions. This work was supported by grants to G.C.P. from the German Science Foundation DFG (FOR 2795/PE1193/6-1) and a DZNE DEMDAS Intersite grant, by grants to A.H. from the Network of Centres of Excellence in Neurodegeneration (CoEN) and a Helmholtz Association Networking Fund, and by grants to F.B. from IRP, WfL, DFG, ERANET AXON REPAIR, and ERANET RATER SCI. F.B. is a member of the excellence cluster ImmunoSensation2 and the SFBs 1089 and 1158, and is a recipient of the Roger de Spoelberch Prize. M.K.S. is a member of the SFB 1089 and SPP 2041.

AUTHOR CONTRIBUTIONS

C.K., C.T., and B.A.T. carried out the experiments and analyzed the data. C.K. and G.C.P. established the methodology, with advice from F.B., M.K.S., and A.H. G.C.P. conceptualized and supervised the study, with input from F.B. G.C.P. wrote the original draft, and C.K. and F.B. edited, commented on, and revised the manuscript.

DECLARATION OF INTERESTS

H. Witte, A. Ertürk, F. Hellal, and F.B. filed a patent on the use of microtubule-stabilizing compounds for the treatment of lesions of CNS axons (European patent no. 1858498; European patent application EP 11 00 9155.0; US patent application 11/908,118).

Received: June 10, 2020
Revised: October 16, 2020
Accepted: November 20, 2020
Published: December 22, 2020

REFERENCES

1. GBD 2016 Stroke Collaborators (2019). Global, regional, and national burden of stroke, 1990-2016: a systematic analysis for the Global Burden of Disease Study 2016. Lancet Neurol. *18*, 439–458.
2. Zerna, C., Thomalla, G., Campbell, B.C.V., Rha, J.H., and Hill, M.D. (2018). Current practice and future directions in the diagnosis and acute treatment of ischaemic stroke. Lancet *392*, 1247–1256.
3. Murphy, T.H., and Corbett, D. (2009). Plasticity during stroke recovery: from synapse to behaviour. Nat. Rev. Neurosci. *10*, 861–872.
4. Stroemer, R.P., Kent, T.A., and Hulsebosch, C.E. (1995). Neocortical neural sprouting, synaptogenesis, and behavioral recovery after neocortical infarction in rats. Stroke *26*, 2135–2144.
5. Napieralski, J.A., Butler, A.K., and Chesselet, M.F. (1996). Anatomical and functional evidence for lesion-specific sprouting of corticostriatal input in the adult rat. J. Comp. Neurol. *373*, 484–497.
6. Carmichael, S.T., Wei, L., Rovainen, C.M., and Woolsey, T.A. (2001). New patterns of intracortical projections after focal cortical stroke. Neurobiol. Dis. *8*, 910–922.
7. Wahl, A.S., Omlor, W., Rubio, J.C., Chen, J.L., Zheng, H., Schröter, A., Gullo, M., Weinmann, O., Kobayashi, K., Helmchen, F., et al. (2014). Neuronal repair. Asynchronous therapy restores motor control by rewiring of the rat corticospinal tract after stroke. Science *344*, 1250–1255.
8. Dancause, N., Barbay, S., Frost, S.B., Plautz, E.J., Chen, D., Zoubina, E.V., Stowe, A.M., and Nudo, R.J. (2005). Extensive cortical rewiring after brain injury. J. Neurosci. *25*, 10167–10179.
9. Carmichael, S.T., Kathirvelu, B., Schweppe, C.A., and Nie, E.H. (2017). Molecular, cellular and functional events in axonal sprouting after stroke. Exp. Neurol. *287*, 384–394.
10. Starkey, M.L., and Schwab, M.E. (2014). How Plastic Is the Brain after a Stroke? Neuroscientist *20*, 359–371.
11. Overman, J.J., Clarkson, A.N., Wanner, I.B., Overman, W.T., Eckstein, I., Maguire, J.L., Dinov, I.D., Toga, A.W., and Carmichael, S.T. (2012). A role for ephrin-A5 in axonal sprouting, recovery, and activity-dependent plasticity after stroke. Proc. Natl. Acad. Sci. USA *109*, E2230–E2239.
12. Joy, M.T., Ben Assayag, E., Shabashov-Stone, D., Liraz-Zaltsman, S., Mazzitelli, J., Arenas, M., Abduljawad, N., Kliper, E., Korczyn, A.D., Thareja, N.S., et al. (2019). CCR5 Is a Therapeutic Target for Recovery after Stroke and Traumatic Brain Injury. Cell *176*, 1143–1157.e13.

13. Ballatore, C., Brunden, K.R., Huryn, D.M., Trojanowski, J.Q., Lee, V.M.Y., and Smith, A.B., 3rd. (2012). Microtubule stabilizing agents as potential treatment for Alzheimer's disease and related neurodegenerative tauopathies. J. Med. Chem. *55*, 8979–8996.

14. Witte, H., Neukirchen, D., and Bradke, F. (2008). Microtubule stabilization specifies initial neuronal polarization. J. Cell Biol. *180*, 619–632.

15. Ertürk, A., Hellal, F., Enes, J., and Bradke, F. (2007). Disorganized microtubules underlie the formation of retraction bulbs and the failure of axonal regeneration. J. Neurosci. *27*, 9169–9180.

16. Hellal, F., Hurtado, A., Ruschel, J., Flynn, K.C., Laskowski, C.J., Umlauf, M., Kapitein, L.C., Strikis, D., Lemmon, V., Bixby, J., et al. (2011). Microtubule stabilization reduces scarring and causes axon regeneration after spinal cord injury. Science *331*, 928–931.

17. Ruschel, J., Hellal, F., Flynn, K.C., Dupraz, S., Elliott, D.A., Tedeschi, A., Bates, M., Sliwinski, C., Brook, G., Dobrindt, K., et al. (2015). Axonal regeneration. Systemic administration of epothilone B promotes axon regeneration after spinal cord injury. Science *348*, 347–352.

18. Cheng, K.L., Bradley, T., and Budman, D.R. (2008). Novel microtubule-targeting agents - the epothilones. Biologics *2*, 789–811.

19. Ruschel, J., and Bradke, F. (2018). Systemic administration of epothilone D improves functional recovery of walking after rat spinal cord contusion injury. Exp. Neurol. *306*, 243–249.

20. Ertürk, A., Mauch, C.P., Hellal, F., Förstner, F., Keck, T., Becker, K., Jährling, N., Steffens, H., Richter, M., Hübener, M., et al. (2011). Three-dimensional imaging of the unsectioned adult spinal cord to assess axon regeneration and glial responses after injury. Nat. Med. *18*, 166–171.

21. Watson, B.D., Dietrich, W.D., Busto, R., Wachtel, M.S., and Ginsberg, M.D. (1985). Induction of reproducible brain infarction by photochemically initiated thrombosis. Ann. Neurol. *17*, 497–504.

22. Schwarz, M.K., Scherbarth, A., Sprengel, R., Engelhardt, J., Theer, P., and Giese, G. (2015). Fluorescent-protein stabilization and high-resolution imaging of cleared, intact mouse brains. PLOS ONE *10*, e0124650.

23. Shanina, E.V., Schallert, T., Witte, O.W., and Redecker, C. (2006). Behavioral recovery from unilateral photothrombotic infarcts of the forelimb sensorimotor cortex in rats: role of the contralateral cortex. Neuroscience *139*, 1495–1506.

24. Liu, Z., Li, Y., Cui, Y., Roberts, C., Lu, M., Wilhelmsson, U., Pekny, M., and Chopp, M. (2014). Beneficial effects of gfap/vimentin reactive astrocytes for axonal remodeling and motor behavioral recovery in mice after stroke. Glia *62*, 2022–2033.

25. Varidaki, A., Hong, Y., and Coffey, E.T. (2018). Repositioning Microtubule Stabilizing Drugs for Brain Disorders. Front. Cell. Neurosci. *12*, 226.

26. Carmichael, S.T., and Chesselet, M.F. (2002). Synchronous neuronal activity is a signal for axonal sprouting after cortical lesions in the adult. J. Neurosci. *22*, 6062–6070.

27. Li, S., Overman, J.J., Katsman, D., Kozlov, S.V., Donnelly, C.J., Twiss, J.L., Giger, R.J., Coppola, G., Geschwind, D.H., and Carmichael, S.T. (2010). An age-related sprouting transcriptome provides molecular control of axonal sprouting after stroke. Nat. Neurosci. *13*, 1496–1504.

28. Dirnagl, U., Hakim, A., Macleod, M., Fisher, M., Howells, D., Alan, S.M., Steinberg, G., Planas, A., Boltze, J., Savitz, S., et al. (2013). A concerted appeal for international cooperation in preclinical stroke research. Stroke *44*, 1754–1760.

29. Colman, H., Nabekura, J., and Lichtman, J.W. (1997). Alterations in synaptic strength preceding axon withdrawal. Science *275*, 356–361.

30. Faul, F., Erdfelder, E., Lang, A.-G., and Buchner, A. (2007). G*Power 3: a flexible statistical power analysis program for the social, behavioral, and biomedical sciences. Behav. Res. Methods *39*, 175–191.

31. Preibisch, S., Saalfeld, S., and Tomancak, P. (2009). Globally optimal stitching of tiled 3D microscopic image acquisitions. Bioinformatics *25*, 1463–1465.

32. Berg, S., Kutra, D., Kroeger, T., Straehle, C.N., Kausler, B.X., Haubold, C., Schiegg, M., Ales, J., Beier, T., Rudy, M., et al. (2019). ilastik: interactive machine learning for (bio)image analysis. Nat. Methods *16*, 1226–1232.

33. Reichenbach, N., Delekate, A., Breithausen, B., Keppler, K., Poll, S., Schulte, T., Peter, J., Plescher, M., Hansen, J.N., Blank, N., et al. (2018). P2Y1 receptor blockade normalizes network dysfunction and cognition in an Alzheimer's disease model. J. Exp. Med. *215*, 1649–1663.

STAR★METHODS

KEY RESOURCES TABLE

REAGENT or RESOURCE	SOURCE	IDENTIFIER
Antibodies		
Anti-GFAP	Dako	Cat#Z0334; RRID: AB_10013382
Anti-Iba1	Wako	Cat#019-19741; RRID: AB_839504
Anti-laminin	Sigma	Cat#L9393; RRID: AB_477163
Anti-fibronectin	Abcam	Cat#ab2413; RRID: AB_2262874
Anti-MBP	Merck	Cat#MAB386; RRID: AB_94975
Anti-ankyrin G	Merck	Cat#MABN466; RRID: AB_2749806
Anti-neurofilament M	Merck	Cat#AB1987; RRID: AB_91201
Anti-SMI312	BioLegend	Cat#837904; RRID: AB_2314902
Anti-CASPR	Abcam	Cat#ab34151; RRID: AB_869934
Anti-NeuN	Merck	Cat#MAB377; RRID: AB_2298772
Alexa Fluor-488 goat anti-rabbit IgG	ThermoFisher	Cat#A11008; RRID: AB_143165
Alexa Fluor-488 goat anti-mouse IgG	ThermoFisher	Cat#A11001; RRID: AB_2534069
Alexa Fluor-594 goat anti-mouse IgG	ThermoFisher	Cat#A11005; RRID: AB_2534073
Alexa Fluor-594 goat anti-rat IgG	ThermoFisher	Cat#A11007; RRID: AB_10561522
Bacterial and Virus Strains		
AAV9.hSyn.eGFP.WPRE.bGH	UPenn Vector Core	Cat#AV-9-PV1696
Chemicals, Peptides, and Recombinant Proteins		
Rose Bengal	Sigma	Cat#330000
Epothilone B	Selleckchem	Cat#S1364
Epothilone D	Abcam	Cat#ab143616
Cholera toxin subunit B Alexa Fluor 594 conjugate	ThermoFisher	Cat#C34777
tert-Butanol	Carl Roth	Cat#AE16.2
Benzyl alcohol	Carl Roth	Cat#0336.2
Benzyl benzoate	Carl Roth	Cat#9498.2
2,2′-Thiodiethanol	Sigma	Cat#166782
Dimethyl sulfoxide	Sigma	Cat#D8418
Triethylamine	Sigma	Cat#T0886
Experimental Models: Organisms/Strains		
Mouse: C57BL/6N	Charles River	RRID: SCR_003792
Software and Algorithms		
ImageJ/Fiji, Version 1.53c	NIH	https://fiji.sc; RRID: SCR_002285
Ilastik toolkit for Fiji	N/A	https://www.ilastik.org/index.html; RRID: SCR_015246
Simple Neurite Tracer (SNT) framework for Fiji	N/A	https://imagej.net/SNT; RRID: SCR_016566
Imaris, Version 9	Oxford Instruments	https://imaris.oxinst.com; RRID: SCR_007370
Prism, Version 8	GraphPad	https://www.graphpad.com/scientific-software/prism/; RRID: SCR_002798
Biorender	Biorender	https://biorender.com; RRID: SCR_018361
G*Power 3	[30])	https://www.gpower.hhu.de; RRID: SCR_013726

(*Continued on next page*)

Continued

REAGENT or RESOURCE	SOURCE	IDENTIFIER
Other		
μ-Dish 50 mm, low	Ibidi	Cat#81136
UMP3 Ultra Micro Pump and Micro4 MicroSyringe Pump controller	WPI	Cat#UMP3-3

RESOURCE AVAILABILITY

Lead Contact

Further information and requests for resources and reagents should be directed to and will be fulfilled by the Lead Contact Gabor C. Petzold (gabor.petzold@dzne.de).

Materials Availability

This study did not generate new unique reagents.

Data and Code Availability

Datasets, custom algorithms and unique code supporting the current study are available from the corresponding author on request.

EXPERIMENTAL MODEL AND SUBJECT DETAILS

All experiments were performed according to animal care guidelines and the ARRIVE criteria. Male C57BL/6N mice (3-5 months old) were purchased from Charles River (Sulzfeld, Germany; RRID: SCR_003792), housed in groups and monitored according to the Federation of European Laboratory Animal Science Associations (FELASA) recommendations under specific pathogen-free conditions. Food and water were provided *ad libitum*, and mice were kept on a 12-h light/dark cycle. All animal research and care procedures were approved by the state's Review Board (Landesamt für Natur, Umwelt und Verbraucherschutz of North Rhine-Westphalia, Germany) and monitored by the responsible veterinary office. 6 animals were excluded from the analysis (two control mice and four mice treated with EpoB died after photothrombosis before reaching the study endpoint). Sample size was predetermined based on a statistical power of 0.8 using G*Power 3 analysis software[30] (RRID:SCR_013726) and based on previous experience.

METHOD DETAILS

Photothrombotic stroke model

Mice were anesthetized by inhalation of isoflurane (3% for induction, 1%–1.5% during surgical procedures, v/v in O_2), and placed in a stereotaxic frame. Body temperature was maintained at 37°C with a heating pad. The skull was circularly thinned by ~50% with a burr drill to a diameter of 1 mm (left hemisphere, 2 mm lateral from bregma). Rose Bengal (30 mg kg^{-1} bodyweight, Sigma) was injected through the tail vein. 5 min after the injection, an optical fiber (Doric Lenses) with an attached LED (515 nm) was placed over the thinned skull, and the region was illuminated for 5 min for cortical blood vessel thrombosis. Following suture, post-operative wound care and analgetic treatment with buprenorphine (0.1 mg/kg; Reckitt Benckiser), mice were placed in a warmed recovery chamber and subsequently transferred into their home cage.

Motor behavior

Mice were individually placed on an elevated grid 50 cm above ground level, and allowed to navigate the grid (30 × 30 cm; grid spacing, 1.3 cm). Videos were taken with a digital camera (Fujifilm Finepix T350). In addition, a mirror was placed underneath the grid to allow videographic capture of foot faults.

Drug treatment

Epothilone B (Selleckchem) or epothilone D (Abcam) were dissolved in dimethyl sulfoxide (DMSO, Sigma), diluted in NaCl and administered intraperitoneally 1 and 15 days after stroke at a concentration of 0.75 mg kg^{-1} bodyweight using a 30G syringe (B. Braun). Control animals received vehicle treatment (DMSO and NaCl without epothilone).

Intracranial injections

For anterograde (AAV9.hSyn.eGFP.WPRE.bGH, UPenn Vector Core) and retrograde (cholera toxin subunit B Alexa Fluor 594 conjugate, ThermoFisher) tracer injections, the following coordinates (stereotactically measured from bregma, in mm) were used: AAV, AP 0.5, ML 1.75, DV 0.5; CTb, AP 2.5, ML 1.5, DV 0.75. Mice were anesthetized using isoflurane (3% for induction, 1%–

1.5% during surgical procedures, v/v in O_2), and body temperature was maintained at 37°C with a heating pad. Injection holes were drilled with a burr drill. Pulled borosilicate capillaries (inner tip diameter, 20 μm; WPI) were mounted on a holder and attached to a syringe (10 μl, Hamilton). Subsequently, the capillary was lowered into the cortex to the target depth, and remained in place for 5 min, followed by the injection at a constant flow rate of 100 nL min^{-1} using a pump (Ultra Micro Pump UMP3 connected to a Micro4 MicroSyringe Pump controller, WPI). After completion, the capillary was kept in place for an additional 5 min to allow for tracer dispersion. Subsequently, injection holes were sealed with bone wax and the skin was sutured. Following post-operative wound care and analgesia, animals were put into a warmed recovery chamber and subsequently transferred to their home cage.

Whole-brain clearing

Whole-brain clearing was based on established protocols.[22] Briefly, fixed mouse brains were washed three times for 5 min in Milli-Q H_2O at room temperature. Subsequently, each brain was transferred to a glass vial (20 ml, Carl Roth) pre-filled with 30% (v/v) tert-Butanol (Carl Roth) solution in Milli-Q at 37°C. The following mixtures, adjusted for the indicated pH values with Triethylamine (Sigma), were used for dehydration/clearing: 30% tert-Butanol (pH 9.9), 50% tert-Butanol (pH 9.7), 70% tert-Butanol (pH 9.5), 80% tert-Butanol (pH 9.6), 96% tert-Butanol (pH 9.5), 100% tert-Butanol (pH 9.4), and BABB (1:2 mixture of benzyl alcohol (Carl Roth) and benzyl benzoate (Carl Roth), pH 9.4). Brains were kept in each dehydration and clearing solution for 1 h at minimal agitation in a 37°C incubator. After tissue dehydration, brains were incubated for 24 h in BABB clearing solution at 37°C to render brains transparent for imaging. Cleared brains were stored protected from light at 4°C.

Immunohistochemistry

Mice were anesthetized with 3% isoflurane in oxygen (v/v) and an intaperitoneal bolus of 1 mg kg^{-1} ketamine. Brains were fixed by perfusion with 15 mL ice-cold 4% (w/v) paraformaldehyde solution and stored overnight at 4°C for post-fixation. Fixed mouse brains were cryo-protected in 15% and 25% (w/v) sucrose solutions (in 1x PBS supplemented with 0.1% (w/v) NaN_3) for 1 day each at 4°C. 20-μm transverse sections were cut with a cryostat (Leica) and stored in 1x PBS supplemented with 0.1% NaN_3 at 4°C. Sections were blocked (1x PBS supplemented with 10% (v/v) normal serum and 0.5% (v/v) Triton X-100) at room temperature for 1 h, and incubated in primary antibody solutions (1x PBS supplemented with 5% (v/v) normal serum and 0.05% (v/v) Triton X-100) overnight at 4°C on a rotating platform (GFAP: 1:250, Z0334, Dako, RRID: AB_10013382; Iba1: 1:250, 019-19741, Wako, RRID: AB_839504; Laminin: 1:25, L9393, Sigma, RRID: AB_477163; Fibronectin: 1:150, ab2413, Abcam, RRID: AB_2262874; MBP: 1:750, MAB386, Merck, RRID: AB_94975; Ankyrin G: 1:100, MABN466, Merck, RRID: AB_2749806; Neurofilament M: 1:100, AB1987, Merck, RRID: AB_91201; SMI312: 1:500, 837904, BioLegend, RRID: AB_2314902; CASPR: 1:750, ab34151, Abcam, RRID: AB_869934; NeuN: 1:100, MAB377, Merck, RRID: AB_2298772). After 24 h, sections were incubated at room temperature for 3 h with Alexa-conjugated secondary antibodies (ThermoFisher; Alexa Fluor-488 goat anti-rabbit IgG, A11008, RRID: AB_143165; Alexa Fluor-488 goat anti-mouse IgG, A11001, RRID: AB_2534069; Alexa Fluor-594 goat anti-mouse IgG, A11005, RRID: AB_2534073; Alexa Fluor-594 goat anti-rat IgG, A11007, RRID: AB_10561522) in 1x PBS. Sections were mounted on a glass microscopy slide with Fluoromount-G medium (supplemented with DAPI; Invitrogen) and stored protected from light.

Confocal and two-photon microscopy

For confocal microscopy, slides were imaged using an upright Zeiss LSM700 microscope. DAPI and Alexa Fluor signals were imaged through 20x (Zeiss, Plan-Apochromat 20x/0.8 M27) or 63x (Zeiss, Plan-Apochromat 63x/1.40 M27) objectives, and saved as 8-bit images. The same image acquisition and filter settings were used for each staining.

Fort two-photon microscopy, BABB-cleared brains were transferred to a metal cylinder with a mirror at the bottom, immersed in clearing solution and placed in a plastic Petri dish (diameter, 10 cm). An imaging dish (μ-dish 50 mm, low; Ibidi) was placed on top of the cylinder and filled with 2,2′-Thiodiethanol (Sigma) to match the refractive index of the clearing solution for two-photon imaging. For all experiments, a 10x objective (Olympus, XLPLN10XSVMP; NA, 0.6; working distance, 8 mm) was attached to a Zeiss LSM 7MP upright two-photon microscope. EGFP signal was detected at 920 nm, and cells positive for Alexa Fluor 594 were detected at 780 nm. Image tile scans and Z stacks were acquired and saved as 8-bit images.

QUANTIFICATION AND STATISTICAL ANALYSIS

All analysis steps were performed by investigators blinded to the group allocation of each dataset. All animals were randomly assigned to experimental groups using the "RAND()" function in Microsoft Excel (RRID: SCR_016137). Sample sizes were determined as described above. Biological replicates for each group are reported in the Figure Legends.

For motor behavior analysis of mice navigating the elevated grid walk test, steps from each paw were counted individually (forepaws, 50 steps; hindpaws, 30 steps) and the number of missteps was used to calculate a paw misplacement ratio for left and right forepaws and hindpaws, respectively.

For the quantification and analysis of neuronal somata positive for CTb conjugated with Alexa Fluor 594, Z stacks were acquired to a depth of 600 μm from the cortical surface. The injection site, as well as regions anterior, medial and lateral from the infarct, or corresponding regions in control mice, were imaged. Positive cells were counted using Fiji (RRID: SCR_002285) after background subtraction, smoothing using a 3D Gaussian blur filter (xy sigma, 5.5; z sigma, 2.0), grayscale conversion and segmentation using a watershed algorithm.

For axonal projection profiles, images were stitched in Fiji using an established algorithm,[31] and subjected to the learning segmentation toolkit ilastik (RRID: SCR_015246)[32] to binarize images according to eGFP signal or background. Subsequently, individual images were registered and verified for consistency of the injection site (Figure S4E). To this end, the area of saturated eGFP signal without visually discernable axons was delineated by a circle and its center was defined as the center of the injection site. Subsequently, images were registered based on anatomical landmarks: to register image stacks of the M1-PMC region, a perpendicular line was drawn from the brain midline to the center of the injection site, and images were excluded from the analysis if the length of this line exceeded 1350 μm ± 10% (based on the AAV injection 1750 μm lateral from midline corrected for 23% isometric tissue shrinkage due to the clearing method[22]; Figure S4E); second, to register stacks of the M1-S1 region, points were drawn at the frontal and caudal end of the lateral brain curvature at Z distances of −50, −150 and −250 μm from surface, respectively, and these points in each plane were connected by a line. Subsequently, another line perpendicular to this line was drawn from the center of the injection site, and images were excluded from the analysis if the length of this line exceeded 1250, 1525 or 1915 μm ± 10% at the three imaging depths (Figure S4E). In the Z direction, stacked images were registered from the cortical surface (z = 0 μm) to a depth of −600 μm. In addition, we quantified the number of eGFP-positive neurons at the injection site (at −100, −150, −200, −250 and −300 μm from surface) and detected no differences between the groups (Figures S4F and S4G). Finally, all maximal projection images from each animal were overlaid in each group, and animals were excluded if the size of the injection site exceeded ± 10% from the mean.

For the analysis of linear structures resembling intact axons, ROIs were placed antero-medially and antero-laterally to the infarct. Linear structures were traced and analyzed using the Simple Neurite Tracer (SNT) framework (RRID: SCR_016566) for Fiji after Hessian-based filtering (sigma, 4.0 pixels).

All ilastik-processed images were registered in Fiji to create a single representation of all axonal projections, and separated into ROIs I-IV. Individual ROIs were loaded into the 3D rendering and analysis software Imaris (Oxford Instruments, RRID: SCR_007370), and axonal projection volumes (expressed in percent distribution) were calculated with the built-in surface creation wizard using thresholds higher than the average background intensity plus the triplicate of the standard deviation. These files were loaded into Imaris to visualize projections.

To quantify axonal coverage at earlier time points, confocal images (XYZ, 900x900x200 μm) were taken from axial brain sections stained for neurofilament M, converted to grayscale images, and binarized using a threshold based on the average background intensity plus the triplicate of the standard deviation, followed by area coverage quantification using Fiji.

To quantify axonal coverage within the red nucleus and facial nucleus, Z stack images of axonal projections into the nuclei were acquired (based on brain atlas coordinates corrected for 23% isometric tissue shrinkage due to the clearing method; red nucleus, 0.6 mm from midline, −3.0 mm from bregma, −2.9 mm from dorsal surface; facial nucleus, 0.9 mm from midline, −4.6 mm from bregma, −4.2 mm from dorsal surface). Two-photon imaging data were binarized in Fiji using a threshold based on the average background intensity plus the duplicate of the standard deviation, followed by area coverage quantification.

Infarct volumes were quantified using Z stack images of the infarct cavity that were analyzed using the built-in surface creation wizard in Imaris.

Immunohistochemical markers (GFAP, Iba1, laminin, fibronectin, NeuN) in the peri-infarct region were quantified in fixed axial brain sections taken at defined time points after stroke using Fiji. To this end, grayscale images were binarized using a threshold based on the average background intensity plus the quadruplicate of the standard deviation, and smoothed using a Gaussian blur (sigma, 2.0), followed by area coverage quantification. NeuN-positive somata were quantified using the Watershed and Analyze Particles plugins in Fiji.

Glial morphology was analyzed in Fiji as described.[33] Briefly, following background removal (automated Huang algorithm; intensity thresholds were calculated based on maximum-intensity projections), 3D particles ($\geq$30 voxels) were reconstructed using a Flood-Filler algorithm, smoothed using a Gaussian filter (sigma, 1.0 px), skeletonized using the Skeletonize3D plugin, and analyzed using the Analyze Skeleton plugin.

Some schematic images were prepared using BioRender (https://biorender.com, RRID: SCR_018361).

We used the Mann-Whitney test for comparisons between two groups, and the Kruskal-Wallis test followed by Dunn's multiple comparisons test or one-way ANOVA followed by Tukey's multiple comparisons test to compare several groups. We used the two-way repeated-measures ANOVA and Bonferroni post hoc test for multiple measurements in the same groups. All data were analyzed using GraphPad Prism 8 (GraphPad Software, RRID: SCR_002798) and are expressed as Tukey's box-and-whisker plots indicating the median, mean, interquartile range (IQR), and 1.5 IQR. A *P value* of less than 0.05 was considered statistically significant. All statistical details are reported in the Figure Legends and Results.